SIZE EFFECTS ON L10 ORDERING IN COPT NANOPARTICLES

by

Darren Wood

Submitted to Brigham Young University in partial fulfillment

of graduation requirements for BS Applied Physics

Department of Physics and Astronomy

Brigham Young University

December 2014

Advisor: Richard Vanfleet

Signature:_____

ABSTRACT

SIZE EFFECTS ON L10 ORDERING IN COPT NANOPARTICLES

Darren Wood

Department of Physics and Astronomy

Bachelor of Science

Analysis of the $L1_0$ order-disorder transition is an area of ongoing research. Current methods of sample preparation, high-resolution imaging, diffraction analysis and energy dispersive X-ray spectroscopy (EDS) analysis were used to analyze samples of 2-12 nm CoPt nanoparticles with the aim of discovering how the order-disorder temperature changes in the shift from the bulk to nano regime. Previous experimentation failed to yield ordered nanoparticles. In response, particles were annealed twice; once to increase size, then to produce ordering. A size increase of 346 % failed to yield ordering.

Funding through National Science Foundation grant DMR-0906385 is gratefully acknowledged.

TABLE OF CONTENTS

List of Figures

CHAPTER 1

Introduction

1.1 Order-disorder phase transition in metallic alloys

Many solid polymetallic alloys typically form a face-centered cubic (fcc) crystal structure (A1 phase), consisting of parallel lattice planes with randomized atomic positions within the structure. Bimetallic alloys such as CoPt can form further ordered arrangements characterized by alternating layers of homogeneous planes ($L1_0$ phase) [1]. At compositions close to 50/50 and below a certain temperature, the $L1_0$ phase is energetically preferred.

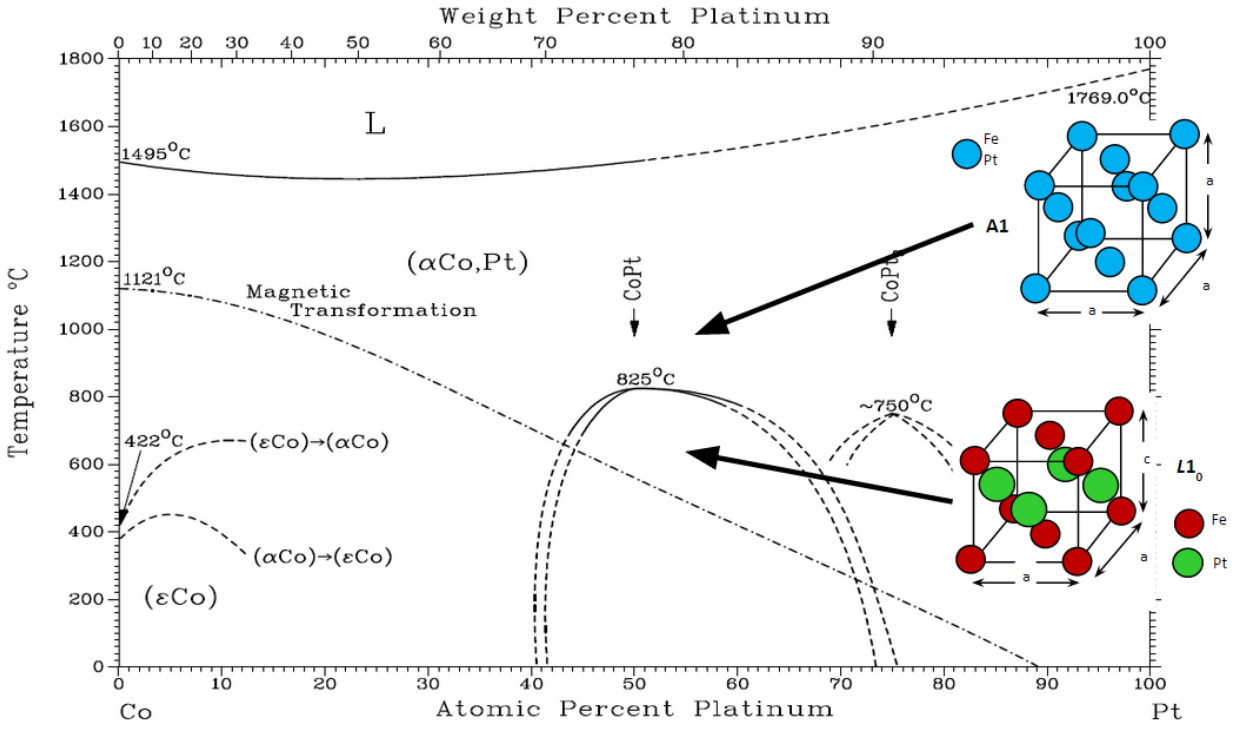

Figure 1: *Phase diagram illustrating order-disorder transition for CoPt*
(Based on an image by Dr. R. Vanfleet) (binary phase diagram taken from [2])

This research focuses on CoPt, which in bulk can take the $L1_0$ phase for Co atomic percentages between 40-73% and temperatures below 825°C (see Figure 1).

1.2 Demand for research in nanomaterials

The $L1_0$ order-disorder phase transition is of major interest in industry and academia because certain interesting phenomena manifest themselves in the ordered $L1_0$ phase. Particularly, ferromagnetic nanoparticles in the $L1_0$ phase have potential application in magnetic recording media [3].

The temperature at which this order-disorder transition occurs has been researched extensively for bulk samples. However, little is known about how this transition behaves in the nano regime. Experimental data is scarce, and theoretical and computational models leave much to be desired. Experiment indicates that in the shift from bulk to thin films, phase transitions such as solid-to-liquid become less abrupt and more gradual [4]. As predicted by computational models [5], the A1-$L1_0$ phase transition should behave similarly as sample size decreases.

Lack of experimental verification is an issue. Conventional hard-disk drives are limited by physical bit size. Currently, one bit of magnetic data storage consists of a field of nanoparticles designed to mitigate data corruption caused by random thermodynamic fluctuations in magnetic dipole moment direction of said nanoparticles. By selecting nanoparticles that are extremely stable with regards to time and temperature, bit size can be reduced exponentially. In order for these ultra-stable particles to be practical, an understanding of their order-disorder transition is necessary. Without research to further this understanding, progress in the area of magnetic recording media is limited.

1.3 Considerations in nanoparticle research

The three factors that most affect nanoparticle ordering are composition, temperature, and size [5]. As shown in Figure 1, particles are most likely to order at compositions of 50/50 CoPt. If compositions are not exactly 50/50, as was the case for our samples, the expected order-disorder temperature must be adjusted. The methods used for adjustment are discussed in Chapter 4.

Temperature is an interesting problem involving the interplay of two related forces: thermodynamics and kinetics. The following energy well drawings assist in explaining how these two factors operate:

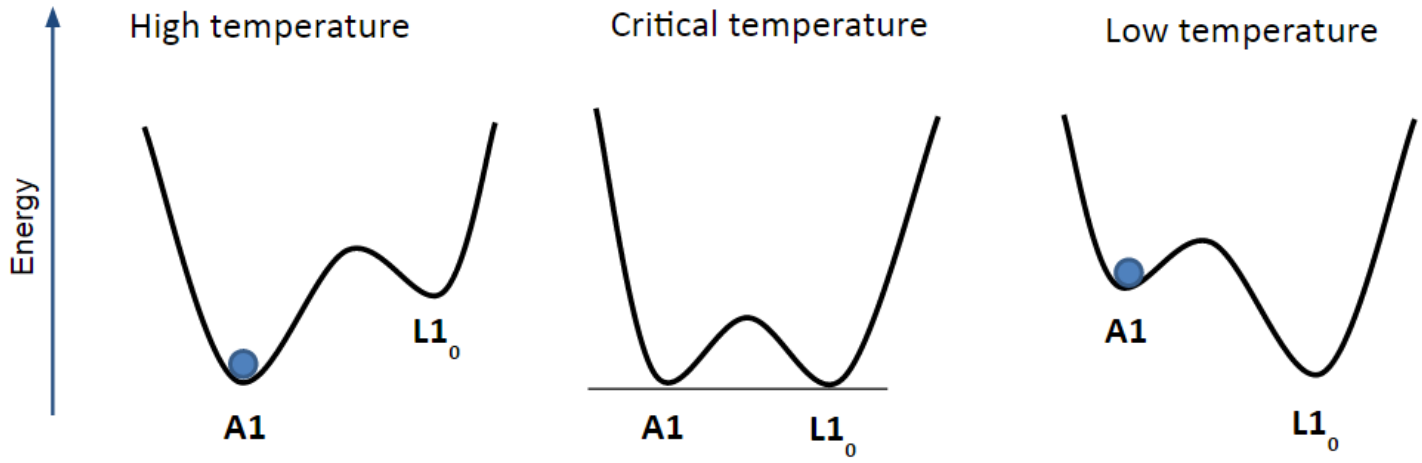

Figure 2: *Energy states of the order ($L1_0$) - disorder (A1) phase transformation (Based on an image by Dr. R. Vanfleet)*

Thermodynamic effects are represented by the depth of the energy wells. At a high temperature, the disordered phase is more favorable to the particle. The lower the temperature, the more the particle "wants" to be ordered. Kinetic effects are represented by the height of the hump in between the two wells. The higher the temperature, the better the particle's chance to cross the hump and move into the other well. Thus, producing ordered nanoparticles becomes a

delicate act of finding the magic temperature that is high enough to give the particle sufficient opportunity (kinetics) while still being low enough to provide sufficient motivation (thermodynamics). To eliminate variations caused by differing temperatures, all of the samples in this project were annealed at the same temperature for the ordering anneal.

The final major consideration and the focus of this paper is particle size. The properties of small samples can be considerably different from the bulk [6]. As sample size decreases, two main effects increase in significance. In the transition from low surface/volume ratio to high surface/volume ratio, surface effects significantly impact thermodynamics [7]. Nucleation also becomes an issue. In a bulk phase transition, when one site in the sample nucleates, the transition can then propagate through the rest of the sample. In the transition from bulk to nanoparticle, the odds of finding a nucleation site decrease proportionally to the total number of atoms. Thus, kinetic considerations are also size dependent. These two factors, along with others, make the study of nanoparticle ordering behavior very difficult, perhaps contributing to the scarcity of research on the topic.

1.4 Development of the project

The intent of this project is to increase the odds of finding $L1_0$ ordered CoPt nanoparticles. Our group's previous work, consisting of annealing 3-6 nm diameter nanoparticles at temperatures near and below the bulk order-disorder temperature, failed to yield ordering. Several avenues presented themselves as options: change anneal temperatures, change compositions, change alloys, change size. We determined that, in light of work being done in parallel with this project, the best course of action would be to increase particle size. This would have the twofold benefit of (a) reducing the surface-to-volume ratio, thereby reducing the strength of surface effects on

thermodynamics and (b) increasing the number of total atoms in each nanoparticle, thereby increasing the odds of finding a nucleation site in a given particle.

CHAPTER 2

Experimental Methods

2.1 Deposition and Annealing

Colleagues at the University of Central Florida (UCF) prepared samples via conventional magnetron sputtering using high-purity Co and Pt targets. Co and Pt were co-sputtered in thin film depositions onto conventional Si wafers with a thin amorphous SiO_2 layer. Volmer-Weber growth produced isolated clusters of atoms in the form of nanoparticles.

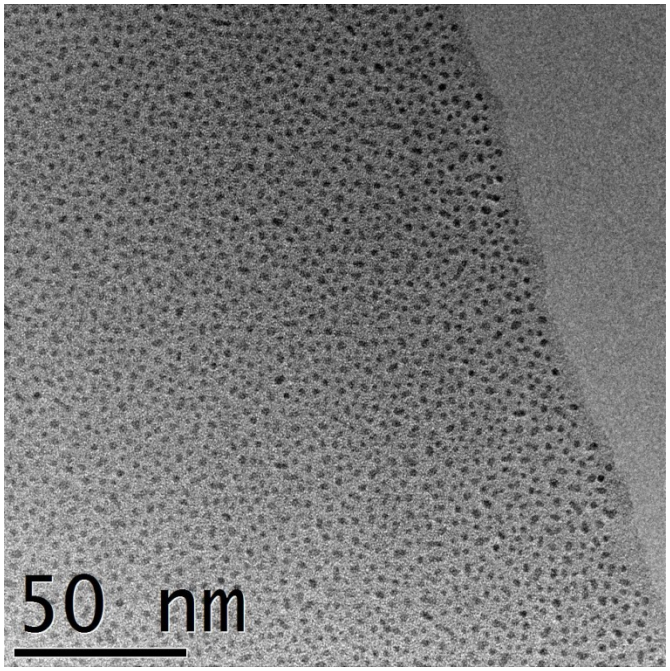

Figure 3: *CoPt nanoparticles, as deposited. Average diameter is 2.11 nm.*

After deposition, the wafers were cleaved into 2 cm by 2 cm pieces and annealed. The samples were annealed in 97 % Ar and 3 % H_2 (addition of H_2 designed to combat the oxidizing effects of

residual H_2O vapor in Ar gas) at 900°C for 30 min to increase size, then at 750°C for 30 min in an attempt to provide the kinetics necessary for ordering.

2.2 Sample Preparation

Analysis in Brigham Young University's FEI Tecnai TF20 analytical scanning transmission electron microscope (STEM) requires samples thin enough to be electron-transparent (thinner than about 100 nm). The sample must also be smooth and as close to atomic level flatness as possible. To achieve this level of sample exactness, tripod polishing was used.

To begin, a 1 mm by 1 mm piece is cleaved from the 2 cm by 2 cm sample wafer using a diamond scribe (Figure 4a). The piece is then washed once in de-ionized water, twice in acetone (C_3H_6O), and once in methanol (CH_4O) (Figure 4b).

(a)

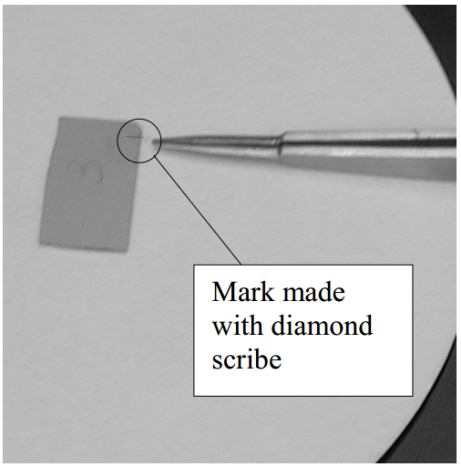

(b)

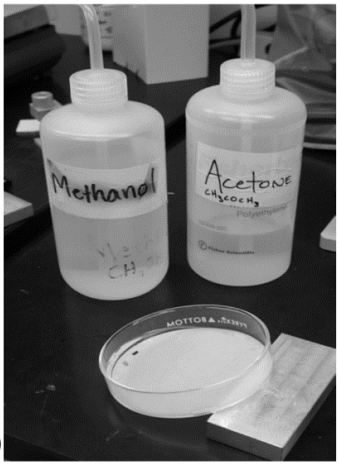

Figure 4: *Cleaving and cleaning a sample in preparation for tripod mounting (Taken from a training manual prepared by Daniel Richardson)*

The piece is then mounted with Crystalbond™ wax to the glass of a tripod polisher with the side containing nanoparticles towards the glass (Figure 5a). The glass will have been polished to 3 μm smoothness prior to mounting.

(a)

(b)

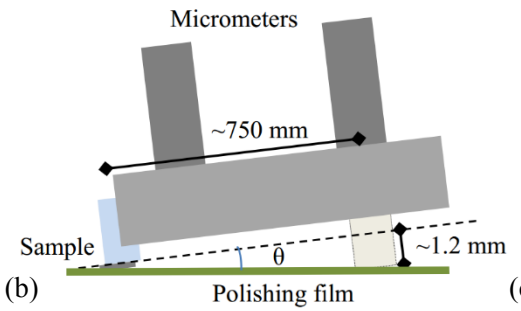

(c)

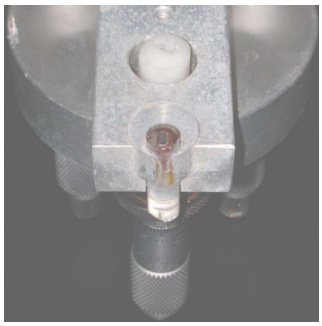

Figure 5: *Tripod polisher setup and micrometer adjustment*
(Taken from a training manual prepared by Andrew Warren)

The rear feet of the tripod are raised to a height of 1.2 mm relative to the sample (Figure 5b), producing a polishing angle of about 0.0016 rad. Heights are measured with a high-precision micrometer (Figure 5c).

After mounting, the sample is polished using successively finer diamond lapping films (Figure 6), followed by 3 minutes of polishing by colloidal silica on a felt pad.

Figure 6: *Tripod polishing setup, with the polisher on the right and the micrometer in the center. Note the multiple diamond lapping films: 30 µm, 6 µm, 3 µm, 1 µm, 0.5 µm.*
(Taken from a training manual prepared by Andrew Warren)

If the colloidal silica step is not done properly, colloidal silica can accumulate on the thin edge of the sample. The silica particles can etch away particles and interfere with TEM analysis, rendering the sample unusable. To prevent colloidal silica infiltration, the preparer must (a) ensure that the layer of wax mounting the sample to the tripod is completely covering the sample, yet very thin, and (b) spin the felt pad at the proper speed to prevent vibration of the sample edge, and (c) keep the felt pad properly lubricated. To remove residual colloidal silica after the polishing step, 5-7 passes are made on a damp Vel-Cloth.

Once the sample reaches an adequate level of smoothness and thinness, it is removed from the tripod polisher with an acetone bath, rinsed in acetone and methanol, and then mounted to a Cu TEM grid with M-Bond™ epoxy. After sitting overnight, the sample and grid are cured on a hot plate at about 110°C for 15 minutes to cure the M-Bond and reduce potential outgassing in the vacuum of the TEM.

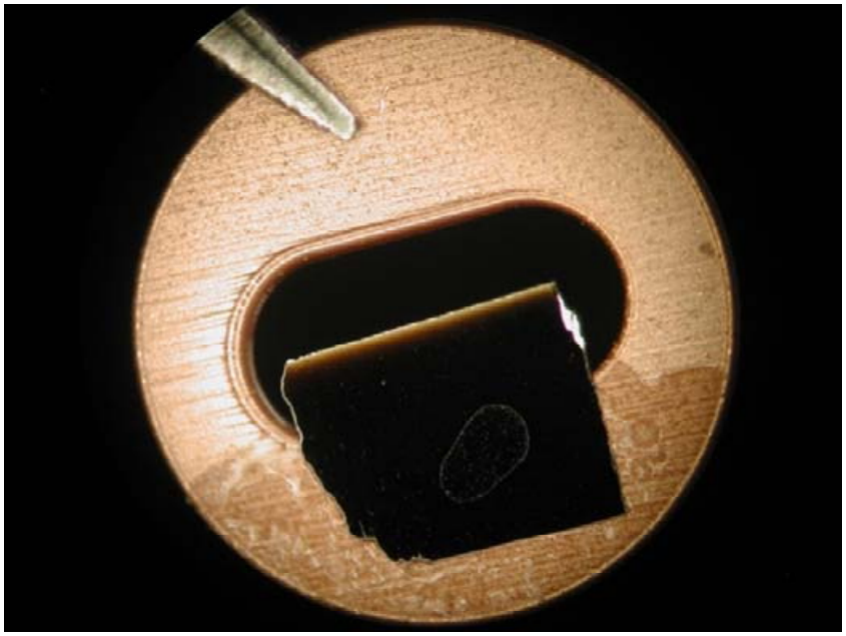

Figure 7: *A polished and mounted TEM sample, ready for analysis.*

2.3 High-Resolution Imaging

A TEM functions according to the same basic principles as a light microscope, using the wave nature of electrons (moving at speeds approaching 0.6 c) instead of the wave nature of light. A motivating voltage of 200 kV (hence the name TF20) is applied to the electron source, known as the "tip." The stream of electrons leaving the tip is transformed into a coherent beam by various magnetic lenses and metal apertures before it reaches the sample. Upon reaching the sample, some of the electrons react with the sample according to the sample density or thickness at a given point, while others are free to pass through. At the bottom of the microscope, the electrons interact with a phosphor screen to produce a "shadow image" of the sample. The different parts of the sample are displayed with varying intensity according to their thickness and density. In our images, the Si substrate appears as a grainy gray color, while the nanoparticles appear as darker, circular objects (Figure 8).

For this thesis, standard conditions for taking size data were 92 kx magnification without lower apertures or sample tilt. Fresnel fringes disappear at the point of exact focus, therefore it is common practice to slightly underfocus when taking high-resolution images to increase contrast [8]. This practice requires experience and judiciousness, however, as an insufficient amount of defocus does not significantly affect resolution, while too much defocus can introduce spurious artifacts into an image to which erroneous significance can be attributed (Figure 8). For our purposes, this "phase contrast focus" sharpened particle edges just enough to provide for accurate size measurements.

Size data was taken by averaging the diameters of all particles within a 100 nm by 100 nm square. An example of a size data spreadsheet is included in Appendix 1.

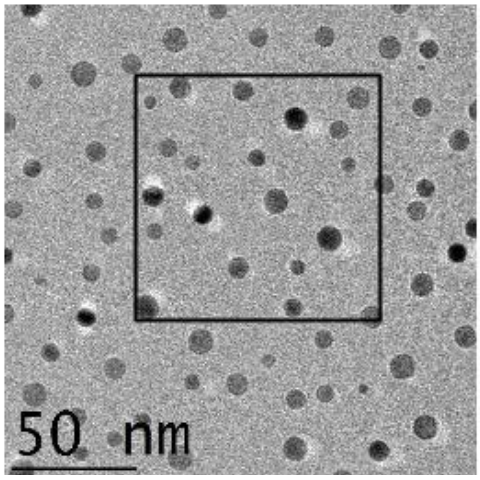

Figure 8: *Double-annealed CoPt nanoparticles photographed at 92 kx magnification. A typical 100 nm by 100 nm box used for size measurements is included. Note the artificial "ghosting" caused by Fresnel contrast underfocus.*

2.4 EDS Spectroscopy

EDS spectra can be used to determine the composition of TEM samples. Figure 9 helps illustrate this. When the TEM's fast electrons interact with the atoms of the sample (event 1), the high-energy beam electrons can excite electrons from the inner orbitals of the atoms. These excited atomic electrons have so much energy that they leave the atom, leaving behind holes that the higher orbital atomic electrons can drop and fill (shown by multiple event 2s). When the higher-energy electrons drop down to lower orbitals, they release energy in the form of x-rays, as illustrated with events 3-5. Each of the different x-ray producing events has a distinct x-ray energy.

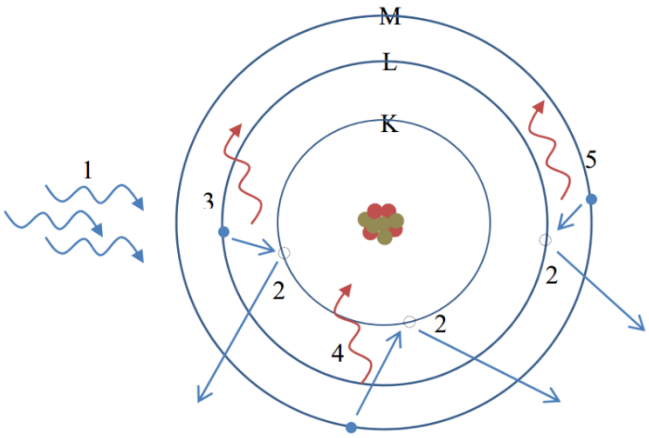

Figure 9: *Illustration of the EDS process. Note the different transitions: 3 - K_α, 4 - K_β, 5 - L_α*

The emitted x-rays are binned according to energy and counted by the EDAX x-ray detector fitted to BYU's TF20. The discreet and unique electron shells in each atom allow for characteristic x-ray energies to be associated with specific electron transitions between specific shells in specific elements [9].

Obtaining quality EDS spectra requires balancing two factors. Too many counts allows multiple x-ray events to overlap in the collection process (giving spurious or broadened peaks) and in extreme cases can damage the x-ray detector. Too few counts leaves the elemental peaks too small to be distinct from background radiation. Figure 10 shows a sample with useable sample-to-background ratios.

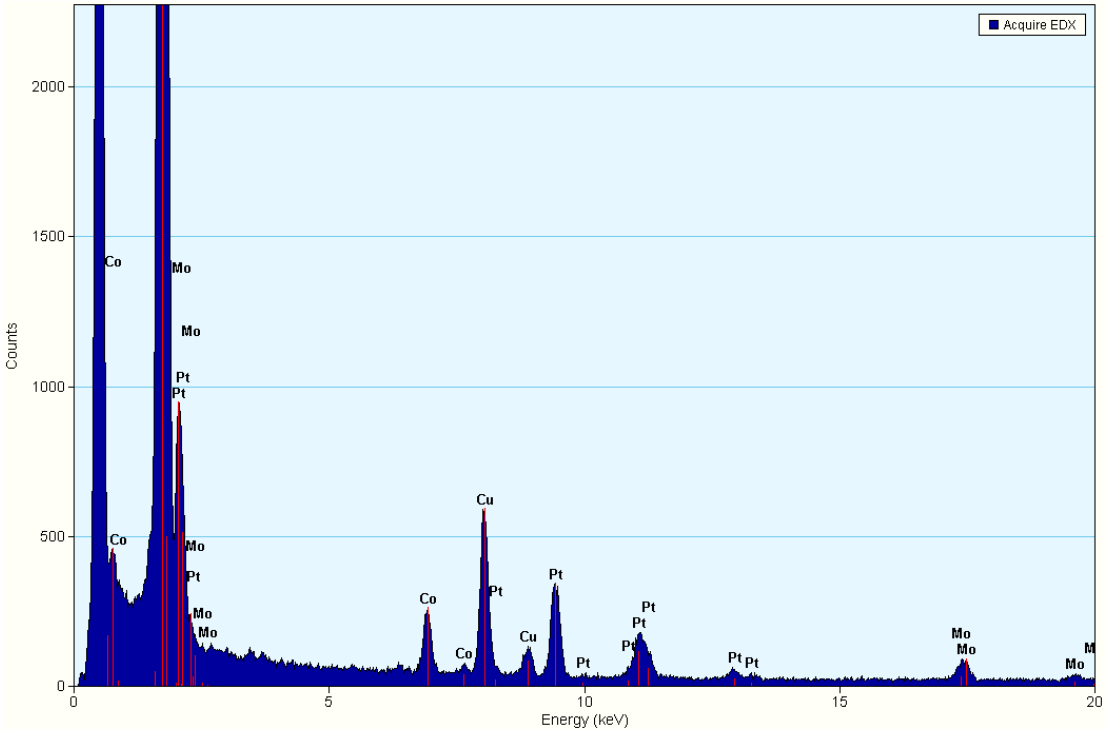

Figure 10: *A typical EDS spectrum for a sample of CoPt nanoparticles. Note the large Si peaks on the left from the sample substrate, the Cu peak in the left-center from the mounting washer, and the Mo peak on the right from the sample holder.*

Count rates can be adjusted by changing the spot size of the electron beam, increasing or decreasing the intensity of the electron beam, or changing position on the sample.

The construction of the microscope itself can affect the spectra taken in two main ways. When a sample sits low in the holder, x-rays are sometimes blocked in their path to the detector. In cases where counts were unusually low, an alpha axis tilt of 15° helped to correct the problem. In addition to this issue, spectra sometimes developed significant peaks at energy levels associated with Fe, even though there was no Fe present in our sample. This is because in BYU's TF20, the sample sits in close proximity to two CoFe pole pieces from a magnetic lens. Under most beam conditions, both stray and deflected electrons can interact with the pole piece

and send extra counts to the x-ray detector. To ensure we weren't including Co counts from the pole piece in our nanoparticle analysis, we needed to account for the extra counts. The TF20 pole pieces are a 50/50 alloy, therefore every Fe count in our spectra corresponded to a non-nanoparticle Co count. To get the true Co count number, we subtracted the number of Fe counts from the total number of Co counts.

Spectra for this project were acquired at count rates between 3 k and 15 k counts/s, depending on beam conditions and sample quality. Integration times ranged from 120 seconds to 180 seconds, depending on count rates (lower rates require more integration time).

2.5 Diffraction Analysis

In the TF20, diffraction patterns can be acquired by passing a collimated electron beam through the sample and viewing the resultant beam in diffraction mode. Even in the A1 disordered state, the periodic face-centered cubic structure of CoPt nanoparticles acts as a diffraction grating, scattering incident electrons in a predictable manner. This interaction can be described by Bragg's Law (note the use of the small angle approximation due to the extremely small wavelength of the incident electrons and resulting small angle of scattered electrons):

$$n\ \lambda = 2\ d\ \mathrm{Sin}(\theta_B) \approx 2\ d\ \mathrm{Tan}(\theta_B) \approx 2\ d \cdot R/2L \qquad 2.1$$

$$\therefore R \propto 1/d \qquad 2.2$$

where λ is the wavelength of the diffracted wave (electron), θ_B is the Bragg angle (half of the angle from the direct beam to the n^{th} diffraction peak), R is the physical distance between the central peak and the n^{th} peak, d is the spacing of the diffraction grating (d-spacing of the nanoparticles' atomic lattice), and L is the distance from the sample to the viewing screen.

The diffraction peaks representing 100 planar periodicity are present in both unordered A1 and $L1_0$. Since diffraction space is reciprocal to real space (Eq. 2.2), closer-spaced diffraction peaks will correspond to larger periodicity in real space (Figure 11).

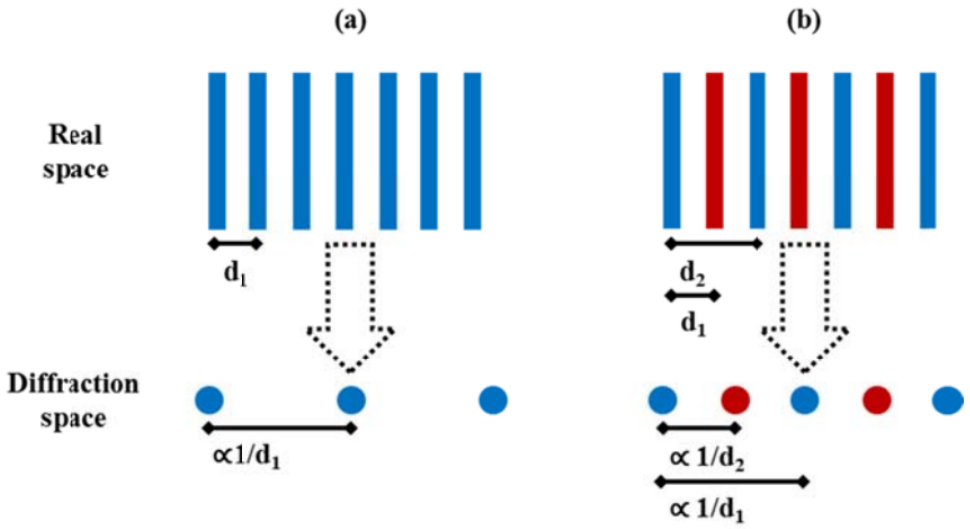

Figure 11: *Illustration of the relationship between real space periodicity and diffraction space peak separation where (a) corresponds to the A1 disordered phase, and (b) corresponds to the $L1_0$ ordered phase*

Diffraction patterns are obtained from multiple particles at once. In order to control the intensity of the pattern, a Selected Area Aperture (sits just below the sample, but in an image equivalent position) was used. Diffraction peaks from an individual particle tend to form a grid-like pattern, indicative of the particle's crystalline structure. When taking a pattern from multiple particles, the different orientations of the particles on the substrate produce several grid patterns rotated around the central peak. This results in an overall diffraction pattern in the form of a series of concentric rings. The radius of each ring corresponds to a particular d-spacing in the sample material.

Since the crystalline Si substrate has only one orientation, it can cause a very strong grid of diffraction peaks if the sample is too thick. If the sample is extremely thin, the crystalline Si

is completely eliminated, leaving only the particles and the SiO_2 layer. In this case, there is no bright Si grid in the diffraction image.

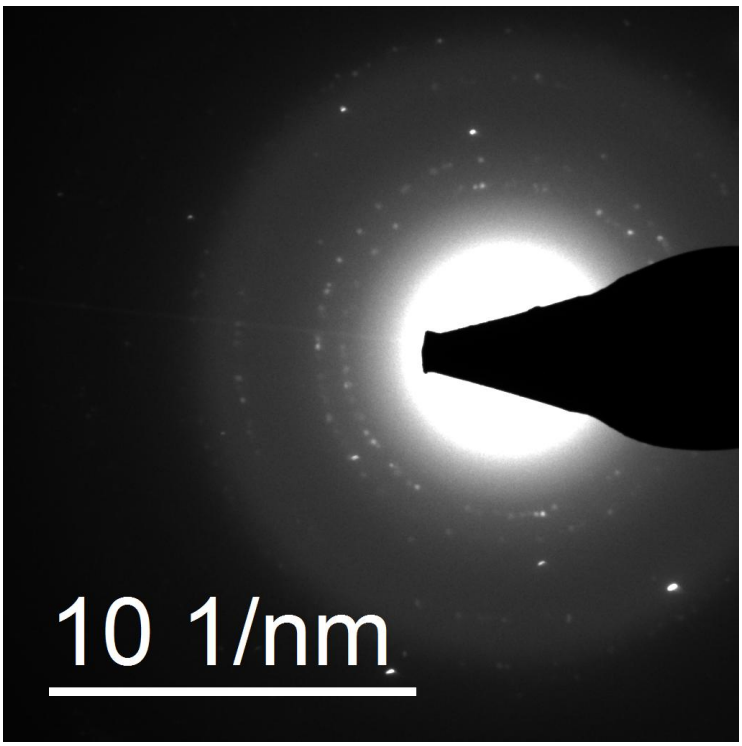

Figure 12: *A typical diffraction image*

Standard conditions for diffraction images in this thesis were a Selected Area Aperture of 40 μm and a camera length of 350 mm.

CHAPTER 3

Experimental Results

3.1 Size Increase

Sputtering produced nanoparticles of average diameters between 2.11 nm and 2.55 nm. Following the size-increasing anneal at 900°C for 30 min and the ordering anneal at 750°C for 30 min, average particle diameter increased to 8.25 nm. The anneal was successful in producing a size increase of 346%.

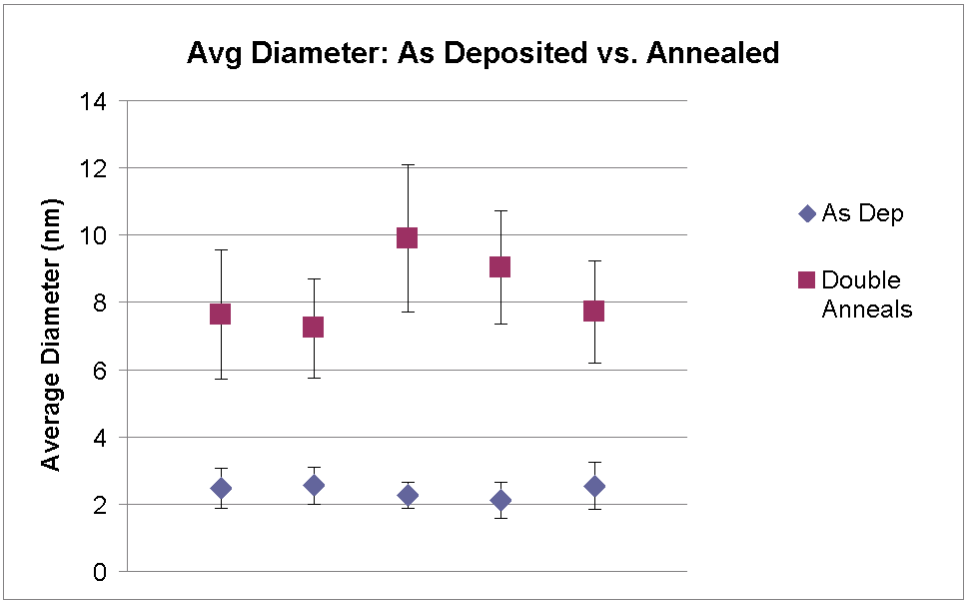

Figure 13: *Sizes of as deposited samples compared with annealed samples*

Average diameter error ranged from as little as 0.38 nm in the as deposited samples to as much as 2.18 nm in the annealed samples. This was due to the known fact that annealed nanoparticles tend to have a broader size distribution [10]. Since diffraction data for this thesis is taken from multiple particles as previously discussed, the variation in particle size is not considered.

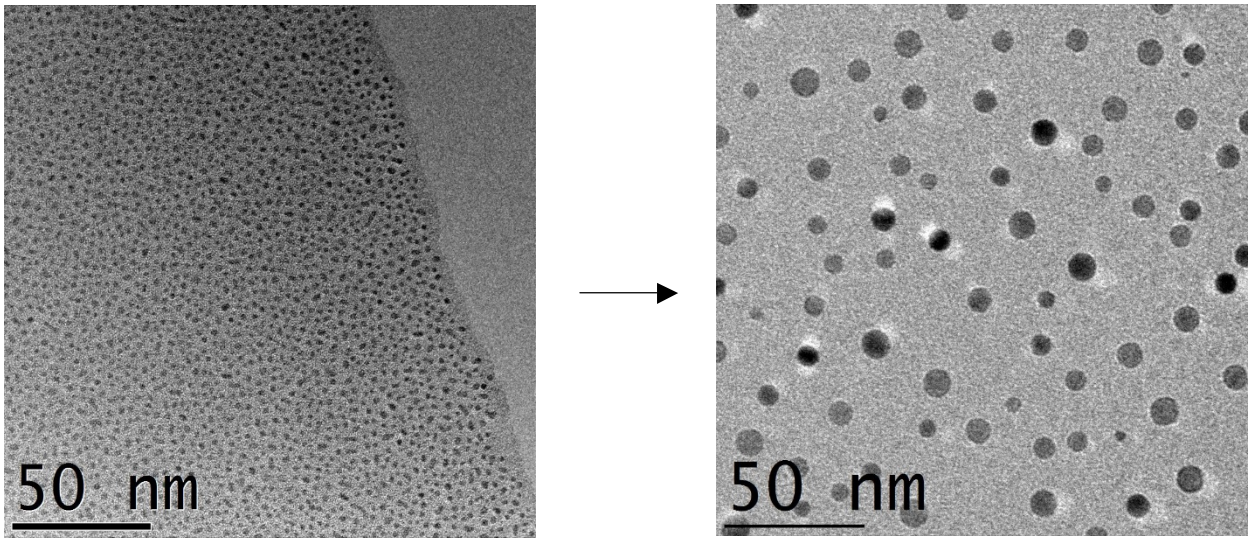

Figure 14: *CoPt nanoparticles before and after the size-increasing anneal*

3.2 Verification of Ordering

5 separate double-anneal samples were analyzed. None of them exhibited ordering. Since this work occurred at the end of my 3 years as a research assistant working with TEM sample preparation and analysis, each of these samples was of high quality. Nanoparticles were found up to the edge of the thin wedges. There was no colloidal silica present, nor was there excessive amounts of Si substrate, both of which have been known to interfere with diffraction images. Over 20 diffraction images were recorded from multiple spots across the five samples, with at

least as many being taken but not recorded due to failure to order. Selected area aperture sizes used ranged from 10 μm to 40 μm to adjust total intensity and diffraction peak density. Not one of these images showed even the faintest of the intermediate peaks indicative of $L1_0$ ordering. Figure 14 compares a typical double anneal CoPt sample with a known ordered FePt sample. The CoPt sample is clearly absent of any rings indicative of ordering.

(a) 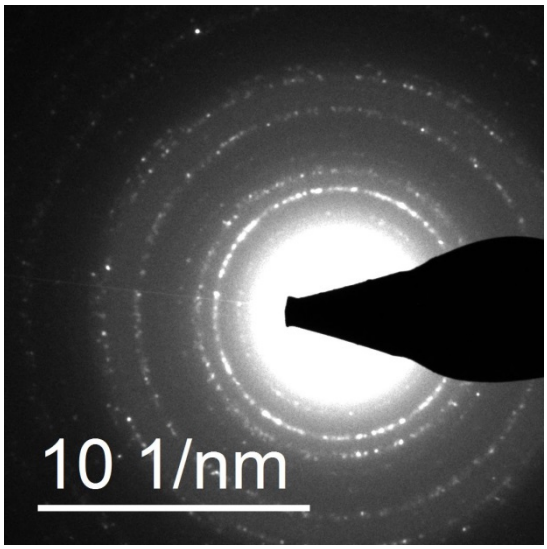

(b) 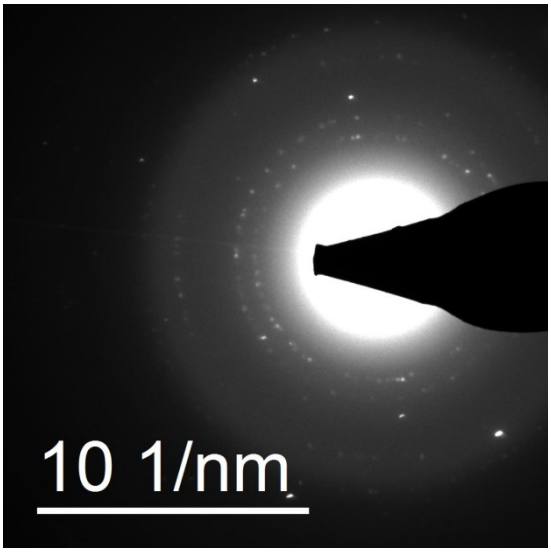

Figure 15: *Comparison of an ordered FePt sample (a) with an unordered CoPt (b). Note that although both samples exhibit the A1 state crystal lattice rings, only the FePt sample exhibits the intermediate rings indicative of $L1_0$ ordering.*

One diffraction image from each of the CoPt samples prepared during the project is included in the appendix for the reader's own examination.

CHAPTER 4

Discussion and Analysis

4.1 Impact of size on order-disorder temperature

Examination of composition data yields possible reasons for the lack of ordering. The three examined samples comprised compositions near 50-50 CoPt, as shown in Figure 15.

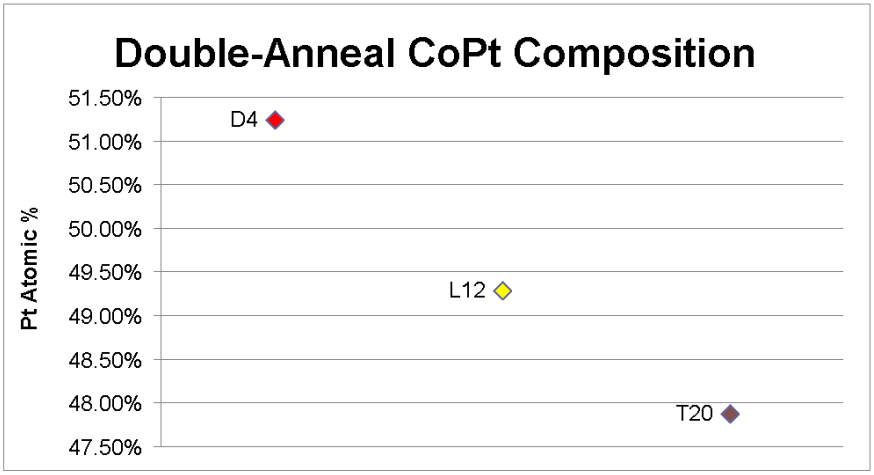

Figure 16: *CoPt sample compositions all fall near 50/50*

Composition affects phase transition temperatures in predictable ways in bulk samples. The order-disorder temperature we had used for our second [ordering] anneal supposes a composition of exactly 50/50. We realized that the fact that our samples weren't exactly 50/50 should change our expectation of the order-disorder temperature. Figure 16 illustrates the method used to find the new expected order-disorder temperature.

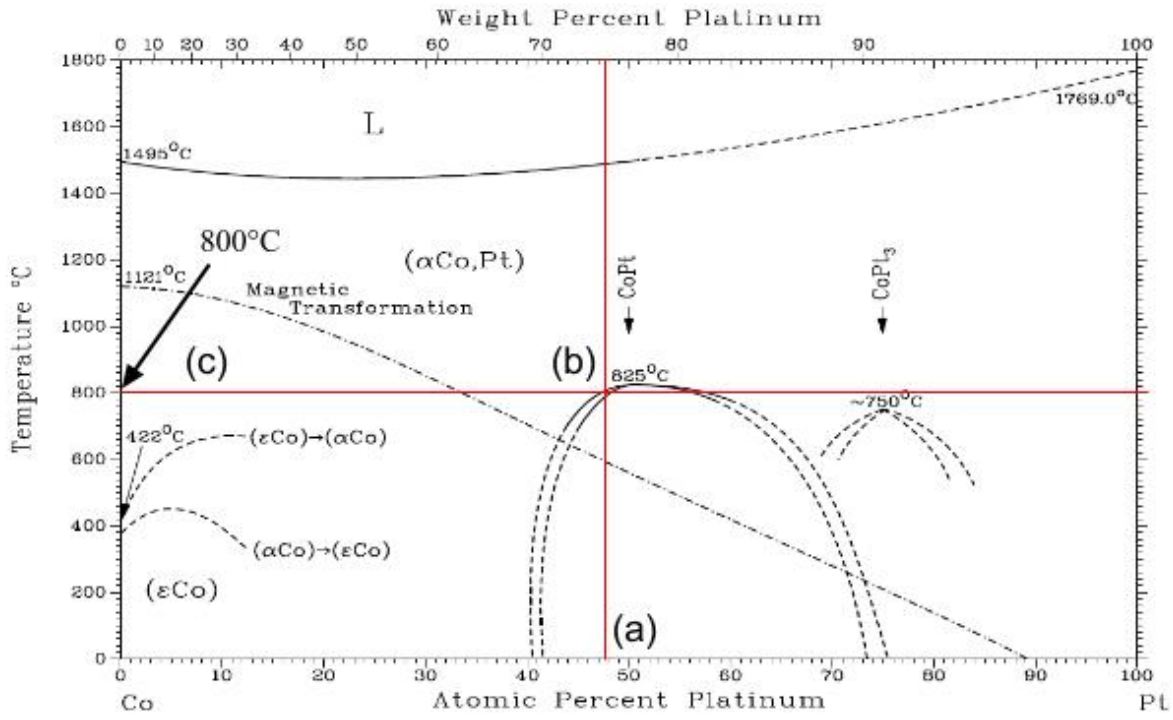

Figure 17: *Phase diagram [11] illustrating the method for finding the new order-disorder temperature for the CoPt sample named T20.*

First, a line is struck from the particle's composition upwards (Figure 16a). Next, a line is struck from the intersection of the first line and the order-disorder curve (Figure 16b). Finally, the new expected order-disorder temperature is read from the left-hand axis (Figure 16c). Using this data, new order-disorder temperatures were found. With the very small variation in sample composition, the maximum shift in order-disorder temperature was only 25 °C, which is not significant for the purposes of this research.

4.2 Failure to Order

Failure of the particles to order suggests 4 main possibilities. Either the kinetics vs. thermodynamics interplay is inherently unfavorable for CoPt, kinetic effects are different in CoPt

than in other similar metal Pt alloys, the order-disorder temperature for nanoparticles of our size dropped much lower from the bulk temperature than expected, or our sample preparation fundamentally inhibited ordering.

It is possible that the kinetics vs. thermodynamics interplay for CoPt nanoparticles is similar to the case of NiPt nanoparticles. $L1_0$ ordering in bulk NiPt samples, although not easy to produce [12] is a well-documented phenomenon [13-14]. Typically, bulk samples are processed in ways that introduce defects that upon annealing aid the ordering process. Since these techniques include cold working, implantation, and long anneals, they are not possible in our nanoparticle synthesis. In our experiments [15], NiPt nanoparticles were unable to exhibit any ordering across a large variation of compositions and anneal temperatures. In performing a search through the literature, any experimental evidence of $L1_0$ ordered NiPt nanoparticles is conspicuously absent. The conclusion to be drawn is that the properties of NiPt nanoparticles are such that the only way to give particles sufficient kinetics to order is to heat them past the point where the ordered state is thermodynamically favorable; therefore no ordering would be seen. It is possible that this is also the case with CoPt. Using FePt as a measure of kinetic needs would indicate that anneals of near 700 °C should be sufficient to allow ordering. In the case of NiPt, the 700 °C value is above the bulk order-disorder temperature and therefore would not achieve ordering. In the case of CoPt, the 825 °C bulk order-disorder temperature is above our anneal temperature and thus should be sufficient unless either (a) FePt is not a good analogy for CoPt kinetic needs or (b) the decrease in CoPt order-disorder temperature with size is significantly greater than expected.

The second possibility is that FePt results are not a good analogy to CoPt in the kinetics regime. K. Barmak et al. [16] used differential scanning calorimetry (DSC) to investigate the A1

to $L1_0$ phase transition in FePt and CoPt thin films. They found that the exothermic peak indicating the A1 to $L1_0$ transition occurs approximately 120 °C lower for FePt than for CoPt films of similar thickness and composition. They concluded that the ordering transformation occurs faster, at a lower temperature, and with a higher magnitude of enthalpy in FePt when compared with CoPt, suggesting that FePt is fundamentally different from CoPt. If this is the case, we should have no reason to believe that just because we got FePt nanoparticles to order, it should be possible to order CoPt nanoparticles under similar conditions.

The third possibility is that the order-disorder temperature dropped much further from the bulk than we expected. In this case, our ordering anneal would have been at a temperature far above the order-disorder temperature. This would clearly never result in ordered particles. Other parties claim to have found the order-disorder temperature of CoPt nanoparticles to be 325 - 175 °C lower than for the bulk [17] for very small particles. If this large critical temperature depression is to be believed, our ordering anneal was much too hot. If this is the case, it would be a simple matter to correct our process to produce $L1_0$ ordered nanoparticles. However, Dr. Vanfleet is suspicious of the logic that led to the conclusion of significant critical temperature lowering in that work. An integral part of their experimental conclusion is the assumption that successful ordering at larger size indicates that a given temperature supplies sufficient kinetics. This neglects the effect of size on the kinetics or ordering, which we believe to be significant.

A final possibility is that the materials surrounding our nanoparticles created an environment that was not conducive to ordering. It is common practice in bulk metallurgy to introduce defects by cold-working samples. Upon annealing, these defects diffuse out of the sample, giving kinetics to the sample and increasing the odds of finding a nucleation site [18].

The nano regime analog of cold-working to produce physical defects is introducing impurities to produce material defects. Outside research that produced successfully $L1_0$ ordered CoPt nanoparticles had one common theme: carbon. In one case, particles were grown on an amorphous carbon film and capped with amorphous alumina (Al_2O_3) [19]. In another, particles were embedded in amorphous carbon [20]. A hypothesis is that the carbon surrounding the particles in those projects acted as a material defect to induce nucleation in the particles. The mobility of carbon through iron is a well-known property that is exploited to great effect in carbon nanotube research [21-22]. It is possible that, upon annealing, the carbon in the substrates diffused through the particles, encouraging ordering. If this is the case, a continuation of this project would include experimentation with carbon substrate or at least a carbon capping layer.

4.3 Discussion of Error

The three primary potential sources of experimental error in this project were inaccuracy of sample processing, inaccuracy of EDS measurements, and improper diffraction methodology.

Error could be introduced in any of the three main steps of the sample preparation process: (a) sputtering, (b) annealing, and (c) polishing. During sputtering, it is possible that certain regions of the sample received disproportionate amounts of Co and Pt in spite of the fact that the elements were sputtered at an atomic percentage ratio of 50/50. This regional variation would account for some of the regional EDS variations on the same sample. In addition, it could produce a field of particles in which no particle was close enough to 50/50 to fall within the $L1_0$ curve of the phase diagram, but the particles taken in aggregate had an overall 50/50 composition. There is also a slight possibility for our particles to exhibit the core-shell behavior

found in other nanoparticles, such as AuCu [23]. This would result in 50/50 overall CoPt particles that nevertheless contain no CoPt atomic alloy. Neither of these situations would produce any ordering. If too much water vapor or impurities were to infiltrate the sample during the annealing process, it is possible that these impurities could react with the Co and shift the sample composition outside of the ordering range shown in Figure 1. Finally, during the polishing process, the colloidal silica could potentially have infiltrated the sample edge and etched part of the particles.

To address possibility (a), several spectra were taken from multiple areas on the same sample, reducing the potential effects of regional variation. Although technically possible in a sputtering deposition situation, core-shell behavior is much more common in chemical reduction deposition. For scenario (b), extra care was taken and high-purity gases were used to ensure pristine anneal environments. For point (c), hundreds of hours of practice and a vigilant monitoring of the sample edge via light microscope during the polishing process minimized the risk.

CHAPTER 5

Conclusion

5.1 Effects of anneal on particle size and order-disorder temperature

The extra anneal of 900 °C for 30 min was successful in enlarging CoPt nanoparticles, increasing average particle diameter 346% from 2.11 nm to 8.25 nm. However, this size increase was not sufficient to produce ordering. Possible reasons include (a) kinetic and thermodynamic limitations making L10 ordering impossible for CoPt nanoparticles (b) kinetic effects are different in CoPt than in other Pt alloys studied, (c) the new 8.25 nm nanoparticles still being sufficiently small as to be so far away from the bulk regime that the order-disorder temperature dropped much more than the we anticipated, and (d) the materials surrounding our nanoparticles created an unfavorable environment for ordering. In the cases of (a) and/or (b), we will have learned about the fundamental physics of CoPt nanoparticles and how they interact with their surroundings. In the case of (c), we will have gathered data points for future nanoparticle research that succeeds in producing ordering. In the case of (d), we will have learned about how CoPt nanoparticles interact with their surroundings.

5.2 Implications for Further Research

If the failure of our particles to order was indeed caused by our annealing temperature being too high, an immediate next step would be to anneal new samples at progressively lower temperatures. If a progression of lower temperatures still yielded no ordering, the next step

would be to experiment with carbon substrates and capping layers, the idea being that carbon's mobility across the ferromagnetic materials would produce defects in the samples and encourage nucleation. If the addition of carbon still does not yield ordering, it would suggest that CoPt can never take the $L1_0$ ordered phase in the nano regime. This would be an interesting development in itself, suggesting that both CoPt and NiPt are somehow fundamentally different from FePt, which orders very consistently in the nano regime. This assertion of difference is supported by calorimetric phase transition studies [24]. This would certainly warrant further exploration into the differences between these three elements that should, by all accounts (ferromagnetism, proximity on the periodic table, etc.), behave very similarly.

Mapping the order-disorder transition of alloyed nanoparticles is the eventual goal of the broader research this project stemmed from. The confirmation of this project of the effects of annealing on nanoparticle size may be used in future research to manipulate particle size and, by extension, order-disorder temperature. In addition, the data gathered by this project will serve as a useful starting point for further exploration into CoPt alloy nanoparticles. At the very least, the work summarized here will provide reasoning to divert focus back to the known-ordering FePt and its associated pseudo-binary alloys.

References

[1] B. Yang, M. Asta, O.N. Mryasov, T.J. Klemmer, R.W. Chantrell, "The Nature of A1—L10 ordering transitions in alloy nanoparticles: A Monte Carlo study", Acta materialia 54:4201-4211 (2006).

[2] P. Villars (ed), H. Okamoto, K. Cenzual, *ASM Alloy Phase Diagram Database*, ASM International, Materials Park 2006-2013.

[3] C.-b. Rong, N. Poudyal, G.S. Chaubey, V. Nandwana, R. Skomski, Y.Q. Wu, M.J. Kramer, and J. Ping Liu, "Structural phase transition and ferromagnetism in monodisperse 3 nm FePt particles", J. Appl. Phys. 102:043913 (2007).

[4] Buschow, K.H.J. (ed). *Handbook of Magnetic Materials, Vol 19*. Elsevier 2011.

[5] C.-b. Rong, D. Li, V. Nandwana, N. Poudyal, Y. Ding, Z.L. Wang, H. Zeng and J.P. Liu, "Size-dependent chemical and magnetic ordering in L10-FePt nanoparticles", Adv. Mater., 18:2984-2988 (2006).

[6] R.R. Vanfleet, J.M. Mochel, "Thermodynamics of melting and freezing in small particles", Surf. Sci., 341(1,2):4050 (1995).

[7] W. Luo, W. Hu, S, Xiao, "Size effect on the thermodynamic properties of silver nanoparticles", J. Phys, Chem. C, 112(7):2359-2369 (2008).

[8] J.M. Cowley, "Image contrast in a transmission scanning electron microscope", Appl. Phys. Lett, 15:58 (1969).

[9] Williams, D.B. *Transmission Electron Microscopy: A Textbook for Materials Science, Vol. IV: Spectrometry.* Springer 2004.

[10] S. Sun, C.B. Murray, D. Weller, L.Folks, A. Moser, "Monodisperse FePt nanoparticles and ferromagnetic FePt nanocrystal superlattices", Science, 17(287)5460:1989-1992 (2000).

[11] P. Villars et al., *ibid*.

[12] U. Kumar, K.G. Padmalekha, P.K. Mukhopadhyay, D. Paudyal, A. Mookerjee, "Magnetic transition in NiPt alloy systems: experiment and theory", J. Magn. Magn. Mater., 292:234-240 (2005).

[13] C.E. Dahmani, M. C. Cadeville, J.M. Sanchez, J.L. Morán-López, "Ni-Pt Phase Diagram: Experiment and Theory", Phys. Rev. Lett. 55:1208 (1985).

[14] C. Leroux, M.C. Cadeville, V Pierron-Bohnes, G. Inden, F. Hinz, "Comparative

investigation of structural and transport properties of $L1_0$ NiPt and CoPt phases; the role of magnetism", J. Phys. F: Met. Phys., 18:2033 (1988).

[15] R.R. Vanfleet, K. Coffey, A. Warren, D. Wood, A. Jackson, unpublished.

[16] K. Barmak, J. Kim, D.C. Berry, W.N. Hanani, K. Weirman, E.B. Svedberg, J.K. Howard, "Calorimetric studies of the A1 to L10 transformation in binary FePt thin films", Appl. Phys. Lett.., 80(22):4268-4270 (2002).

[17] D. Alloyeau, C. Ricolleau, C. Mottet, T. Oikawa, C. Langlois, Y. Le Bouar, N. Braidy, A. Loiseau, "Size and shape effects on the order-disorder phase transition in CoPt nanoparticles", Nat. Mat., 8:940-946 (2009).

[18] T.J. Klemmer, C. Liu, N. Shukla, X.W. Wu, D. Weller, M. Tanase, D.E. Laughlin, W.A. Soffa, "Combined reactions associated with $L1_0$ ordering", J. Magn. Magn. Mater., 266:79-87 (2003).

[19] D. Alloyeau et. al., *ibid*.

[20] F. Tournus, A. Tamion, N. Blanc, A. Hannour, L. Bardotti, B. Prével, P. Ohresser, E. Bonet, T. Epicier, V. Dupuis, "Evidence of $L1_0$ chemical order in CoPt nanoclusters: direct observation and magnetic signature", Phys. Rev. B 77:144411 (2008).

[21] H. Yoshida, S. Takeda, T. Uchiyama, H. Kohno, Y. Homma, "Atomic-Scale In-situ Observation of Carbon Nanotube Growth from Solid State Iron Carbide Nanoparticles", Nano Lett., 8(7):2082-2086 (2008)

[22] K. Moulton, N.B. Morrill, A.M. Konneker, B.D. Jensen, R.R. Vanfleet, D.D. Allred, R.C. Davis, "Effect of iron catalyst thickness on vertically aligned carbon nanotube forest straightness for CNT-MEMS", J. Micromech. Microeng., 22(5):055004 (2012).

[23] J.A. Ascencio, H.B. Liu, U. Pal, A. Medina, Z.L. Wang, "Transmission electron microscopy and theoretical analysis of AuCu nanoparticles: Atomic distribution and dynamic behavior", Micr. Res. Techn., 69(7):522-530 (2006).

[24] K. Barmak et al., *ibid*.

Appendix 1

An example of the spreadsheets used for size analysis.

	A	B	C	D	E	F	G
1		**Particle Diameter**	**Square Side Length (nm)**	**# of Particles**			
2		6.3	100.05	30			
3		6.84					
4		4.96					
5		8.95					
6		6.71					
7		6			**Sample**	**Average Diameter**	**Distribution (Particles per nm squared)**
8		9.28			Two Stage Anneal: 900C then 750C	7.235	0.002997002
9		6.85				**Avg. Diam. Error**	**Equivalent Thickness**
10		9.84				1.477440129	0.594293934
11		8.6					
12		5.36					
13		6.78					
14		7.62					
15		8.08					
16		8.27					
17		8.38					
18		5.12					
19		6.37					
20		7.07					
21		7.41					
22		5.62					
23		5.29					
24		6.86					
25		9.52					
26		9.35					
27		**5.83**					
28		6.28					
29		8.23					
30		7.34					
31		7.94					
32							

Appendix 2

A comparison of a known ordered FePt diffraction image with a characteristic diffraction image from each sample examined in this thesis.

Ordered FePt

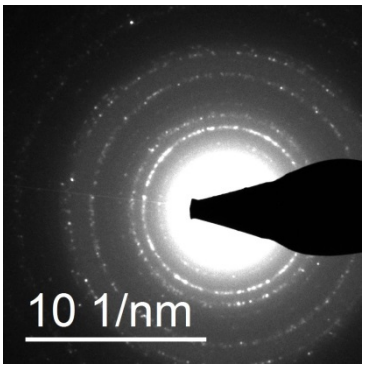

Disordered CoPt sample A1

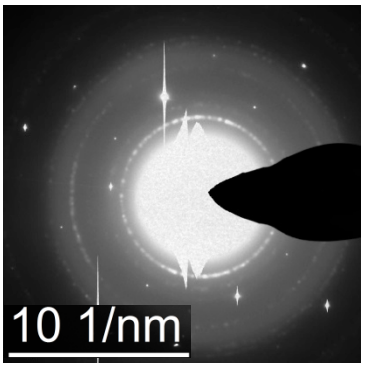

Disordered CoPt sample D4

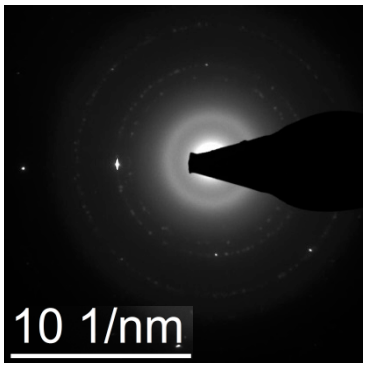

Disordered CoPt sample G7

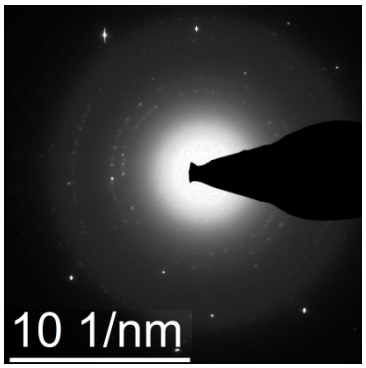

Disordered CoPt sample L12

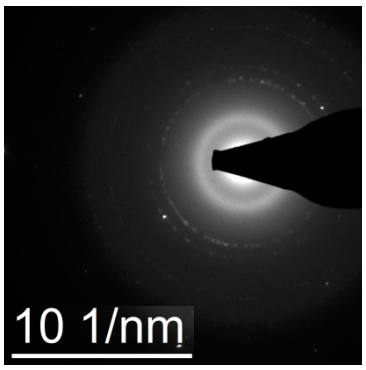

Disordered CoPt sample T20